Ceramics International 48 (2022) 9477–9482

Contents lists available at ScienceDirect

Ceramics International

journal homepage: www.elsevier.com/locate/ceramint

Morphology and surface engineering of vertical graphene films for dye photodegradation

Jin Ren [a,1], Jiemin Han [a,1], Yifei Ma [a,*], Mei Wang [a,**], Zhaomin Tong [a], Jonghwan Suhr [b], Liantuan Xiao [a], Suotang Jia [a], Xuyuan Chen [a,c]

[a] State Key Laboratory of Quantum Optics and Quantum Optics Devices, Institute of Laser Spectroscopy, Collaborative Innovation Center of Extreme Optics, Shanxi University, Taiyuan, 030006, China
[b] Department of Polymer Science and Engineering, School of Mechanical Engineering, Sungkyunkwan University, Suwon, 16419, Republic of Korea
[c] Faculty of Technology, Natural Sciences and Maritime Sciences, Department of Microsystems, University of Southeast Norway, Borre, N3184, Norway

ARTICLE INFO

Keywords:
Vertical graphene
PECVD
Surface engineering
Photodegradation performance

ABSTRACT

It has been reported that vertical graphene (VG) has the capability to be a photocatalyst. In previous studies, the morphology evolution of the VG films synthesized by the plasma-enhanced chemical vapor deposition (PECVD) process has been investigated. This work focuses on the impact of the morphologies of the VG films on photocatalytic properties. Three morphologies of the VG films, VG with porous graphene (VG-P), 'forest-like' graphene (VG-F), and 'wall-like' vertical graphene (VG-W), are fabricated and the photodegradation properties are investigated. In order to enhance the photodegradation property of the VG films, the surface of the VG films with different morphologies is treated with oxygen plasma, in which the oxygen plasma treated VG-P, VG-F, and VG-W are named as VG-P-O, VG-F-O, and VG-W-O, respectively. As a result, the VG-P-O shows the best degradation performance of 82.6% for methylene blue and 86.7% for methyl orange, which is attributed to the desirable porous structure and the modified hydrophilicity.

1. Introduction

Graphene has become a promising material in the field of photocatalysis due to its prominent electrical conductivity [1], high carrier mobility at room temperature [2], large specific surface area [3], and easy modification of the surface functional groups [4]. However, the graphene-based materials encounter the challenge of self-restacking derived from the high surface energy. The vertical graphene (VG) can avoid the restacking issues through the vertical growth of the graphene sheets [5]. It has been demonstrated that the vertical graphene nanowalls can efficiently adsorb the sunlight, separate the photo-generated charge carrier and promote the charge transport, which are the most important features of the photocatalysts [6].

Accordingly, Guirguis et al. has successfully prepared the vertically aligned graphene nanosheets and accomplished the photocatalytic dye degradation, proving that the VG has the ability to be as a photocatalyst [5]. However, for carbon materials, the surface morphology and structure significantly affect their properties. For example, Brownson et al. reported that the taller VG structures provided better heterogeneous electron transfer rates, demonstrating that the edge plane sites are the primary source of electron transfer in carbon materials [7]. Ghosh and coworkers tuned the gap between the vertically aligned graphene nanosheets to control the hydrophilic property with the contact angle from 103° to 135° [8]. Besides, the doping of heteroatoms also has a crucial influence on the properties of VG. Li's group reported that the nitrogen-doped vertical graphene exhibited enhanced hydrogen evolution reaction performances due to the enlarged surface area and optimized electronic structure due to the introduction of nitrogen heteroatoms [9]. These works indicate that the VG possesses photocatalytic properties, yet it's not clear whether the morphology affects the photocatalytic performances.

In this study, we focus on the impact of the morphology on the photocatalytic properties of the VG films. Three morphologies of the VG films, porous graphene, 'wall-like' graphene, and 'forest-like' graphene, are fabricated via the plasma-enhanced chemical vapor deposition (PECVD) process by controlling the growth conditions. The structure-

* Corresponding author.
** Corresponding author.
E-mail addresses: mayifei@sxu.edu.cn (Y. Ma), wangmei@sxu.edu.cn (M. Wang).
[1] These authors contribute equally to this work.

https://doi.org/10.1016/j.ceramint.2021.12.145
Received 26 November 2021; Received in revised form 13 December 2021; Accepted 14 December 2021
Available online 18 December 2021

Table 1
Growth conditions of the VG films with different morphologies.

	Growth Time (min)	Temperature (°C)	Plasma Power (W)
VG-P	60	700	280
VG-F	60	800	280
VG-W	60	700	120

photodegradation relationship of the VG films is investigated towards the degradation of organic dyes, methylene blue (MB) and methyl orange (MO), under the ultra-violet (UV) stimuli. As a result, the porous graphene shows the highest degradation rate of 75.0% for MB and 83.4% for MO. Further surface treatment by oxygen plasma is applied to append oxygen-containing functional groups on the VG nanosheets, which ameliorates its hydrophilicity and enhances the photocatalytic properties. With the demonstrated relationship between the morphology and the photocatalytic capabilities of the VG films, we believe that the properties of the VG films can be effectively controlled by adjusting the morphologies, demonstrating the broader application adaptability of the VG films.

2. Materials and methods

2.1. Preparation of the VG films

The VG films with different morphologies were prepared by a PECVD process as reported in previous studies [10–13]. In brief, a quartz of 1 × 1 cm^2 was used as the substrate and located in the heating area of a tube-type inductive coupled PECVD system. A mixture of H_2 and C_2H_2 were used as precursors at a flow rate of 3 and 1 sccm, respectively. Then, the VG with porous structure (VG-P), 'wall-like' vertical graphene (VG-W), and 'forest-like' graphene (VG-F) were synthesized at different conditions as listed in Table 1.

Furthermore, the oxygen-treated VG films were also prepared. The VG films with different morphologies were treated with oxygen plasma under the O_2 flow rate of 3 sccm for 4 min at room temperature in PECVD. Accordingly, the VG-P, VG-F, and VG-W after oxygen plasma treatment were named VG-P-O, VG-F-O, and VG-W-O, respectively.

2.2. Photocatalytic degradation

Cationic (MB, 90%, Aladdin Co.) and anionic (MO, 96%, Aladdin Co.) dyes with the concentration of 5 mg L^{-1} were prepared as organic pollutants for photocatalytic degradation. Firstly, the VG catalyst was immersed in 3 mL of dye solution for 30 min to reach an equilibrium of adsorption/desorption in darkness. Then, the solution was exposed under the ultraviolet light source of 365 nm at a power density of 180 mW cm^{-2} for 240 min, during which the absorbance of the solution was measured every 10 min. The blank controller was conducted following the above process without the VG catalyst.

2.3. Characterizations

The morphology and microstructure were observed by a scanning electron microscope (SEM, HITACHI, SU-8010). Raman spectra were recorded on a Horiba Scientific LabRAM HR Evolution with a laser operating at 532 nm. The static contact angles were measured by dropping 5 μL of water droplets on the VG surfaces through a syringe device and analyzed by a digital goniometer (KRÜSS, DSA25B). The absorbance was measured with an Ultraviolet–Visible-near-IR Spectroscopy (UV–Vis–NIR, PerkinElmer Lambda 1050+).

Standard curves of concentration vs. absorbance of dye solution were measured according to the Beer's Law and shown in Fig. S1. MB and MO solutions with different concentrations (0.1, 0.2, 0.5, 0.8, 1, 2, and 5 mg L^{-1}) were prepared. The maximum value of the absorbance at the wavelengths of 675 nm for MB and 479 nm for MO were measured to plot the standard curves. Accordingly, the equation of standard curves was calculated as follows:

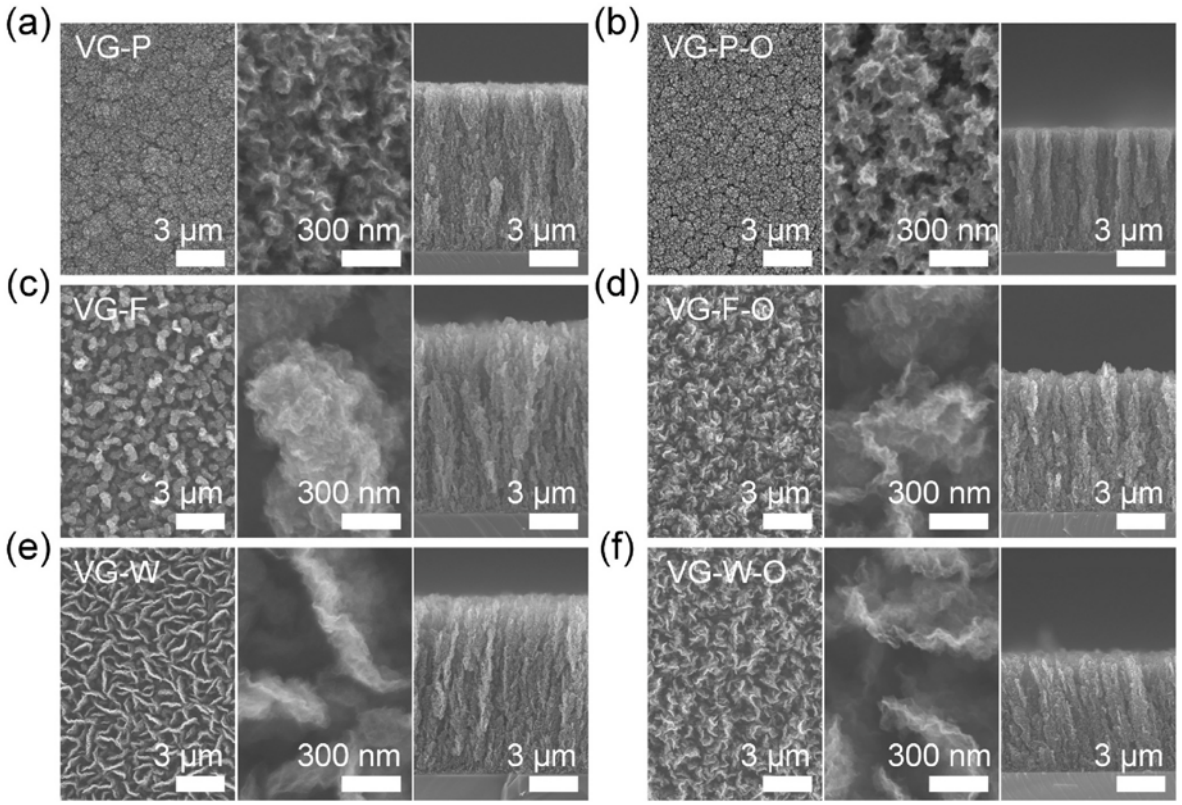

Fig. 1. Top-view and cross-sectional SEM images of the VG-P (a), VG-P-O (b), VG-F (c), VG-F-O (d), VG-W (e), and VG-W-O (f).

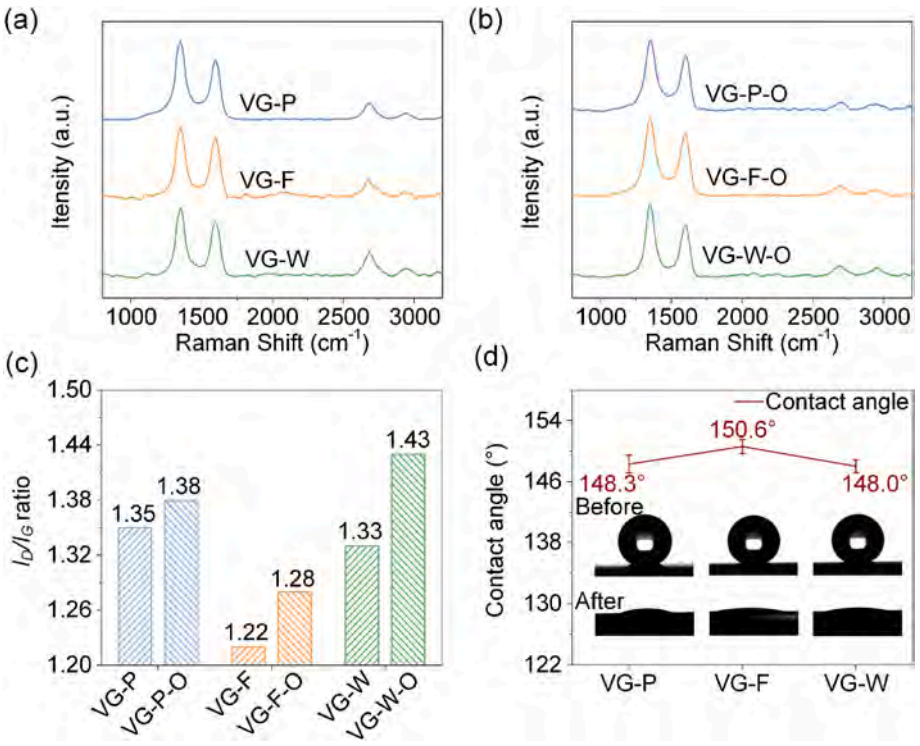

Fig. 2. The Raman spectra of the VG films before (a) and after (b) oxygen treatment. The I_D/I_G value changes of VG films before and after oxygen etching (c). Contact angles of the VG films before and after oxygen etching (d).

MB: $A = 0.26625C - 0.00644$

MO : $A = 0.06896C - 0.02804$

where the C is the concentration (mg L^{-1}), and the A is absorbance. The photodegradation efficiency was calculated using the following equation:

$$\eta(\%) = -(C - C_0) / C_0 \times 100$$

where the η is the photodegradation efficiency, the C is the current concentration (mg L^{-1}), and the C_0 is the initial concentration (mg L^{-1}). In addition, the photodegradation rate K (min^{-1}) was calculated using the following equation:

$$K \times t = -ln(C / C_0)$$

where the t is degradation time (min).

Besides, the half-life time value was calculated from the K, as the following equation [5]:

$$t_{1/2} = ln(2)/K$$

where the $t_{1/2}$ is the half-life time of the degradation process.

3. Results and discussion

3.1. Structural characterizations

Morphologies of the VG films before and after oxygen plasma treatment are illustrated in Fig. 1a–f. The obvious morphology differences of the VG-P, VG-F, and VG-W in Fig. 1a, 1c, and 1e indicate the morphology of the VG films is successfully steered by controlling the deposition conditions during the PECVD process. The VG-P shows a porous structure with a compact pileup of small graphene nanosheets (Fig. 1a). The VG-F presents a 'forest-like' structure with the graphene nanosheets packed into graphene 'trees' because of the high density and activities of the ions and radicals derived from the high temperature and plasma power (Fig. 1c). And the VG-W shows a morphology with randomly and vertically aligned graphene microflakes (Fig. 1e). It is worth noting that the height of the VG films is cut down after the oxygen plasma treatment while the cross-sectional morphology does not change obviously (Fig. 1b, 1d, 1f and Table S1). However, the top-view morphologies of the VG-F and VG-W change on the surface, that is, the top surface of the VG flakes is dependently and vertically oriented other than conglobated. During the oxygen treatment, the top clusters of the VG-F and VG-W are etched into small flakes while maintaining the initial cross-sectional structure.

The crystalline structure of the VG films is further characterized by Raman spectroscopy. As depicted in Fig. 2a and b, peaks at 1348, 1600, and 2683 cm^{-1} are obtained corresponding to the typical D, G, and 2D peaks of graphene. The graphitic crystalline structure of the VG can also be demonstrated by the transmission electron microscopy (TEM) characterizations in our previous studies [12,14]. Generally, the integrated intensity ratio of the D to G peaks (I_D/I_G) is used to show the imperfection of carbon materials, that is, a larger I_D/I_G value indicates a higher defect level. In the PECVD process, reactions are complex that the active radicals and ions synergistically work in a balance of the etching and deposition effects [14]. As a result, strong D peaks are observed in the VG-P, VG-F, and VG-W, which are induced by the etching effect. More defects are induced after the oxygen treatment that the I_D/I_G ratios are increased in the VG-P-O, VG-F-O, and VG-W-O, as presented in Fig. 2c.

A better hydrophilic property of the VG films can benefit the accessibility of the pollution to the surface of the graphene flakes. Thus, the contact angles of the VG films with different morphologies are evaluated in Fig. 2d. Graphene has an intrinsic contact angle of 85°–90° [15]. Owing to the exposed sharp edges [16], all the VG films exhibit an ultra-high hydrophobic property that the water drop shows a mellow droplet shape on the VG film surface with contact angles over 148°. However, after the oxygen functional groups and defects are induced to the VG films by the oxygen plasma treatment, a great decrease of the contact angles occurs that the water drop infiltrates the VG films

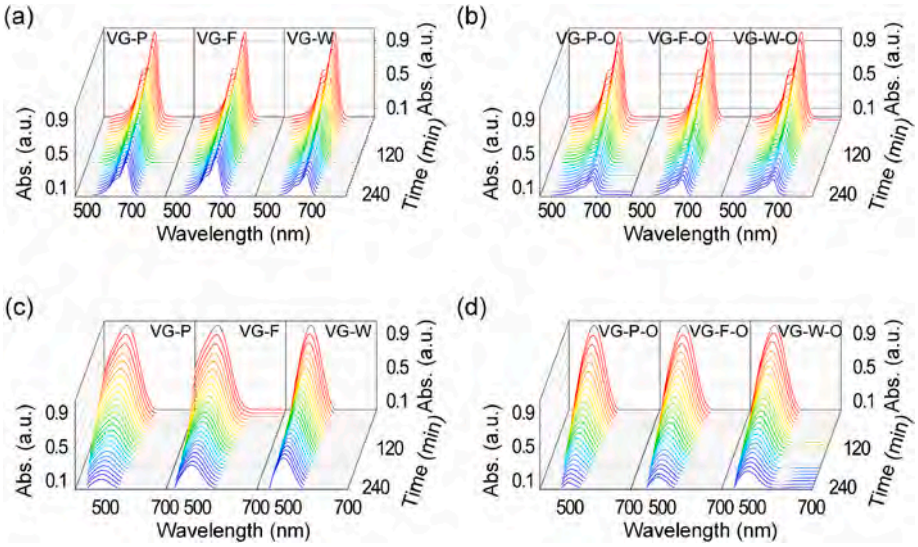

Fig. 3. The absorbance variation of the MB solution over time with the photocatalysis of VG films before (a) and after (b) oxygen treatment. The absorbance variation of the MO solution over time with the photocatalysis of VG films before (c) and after (d) oxygen treatment.

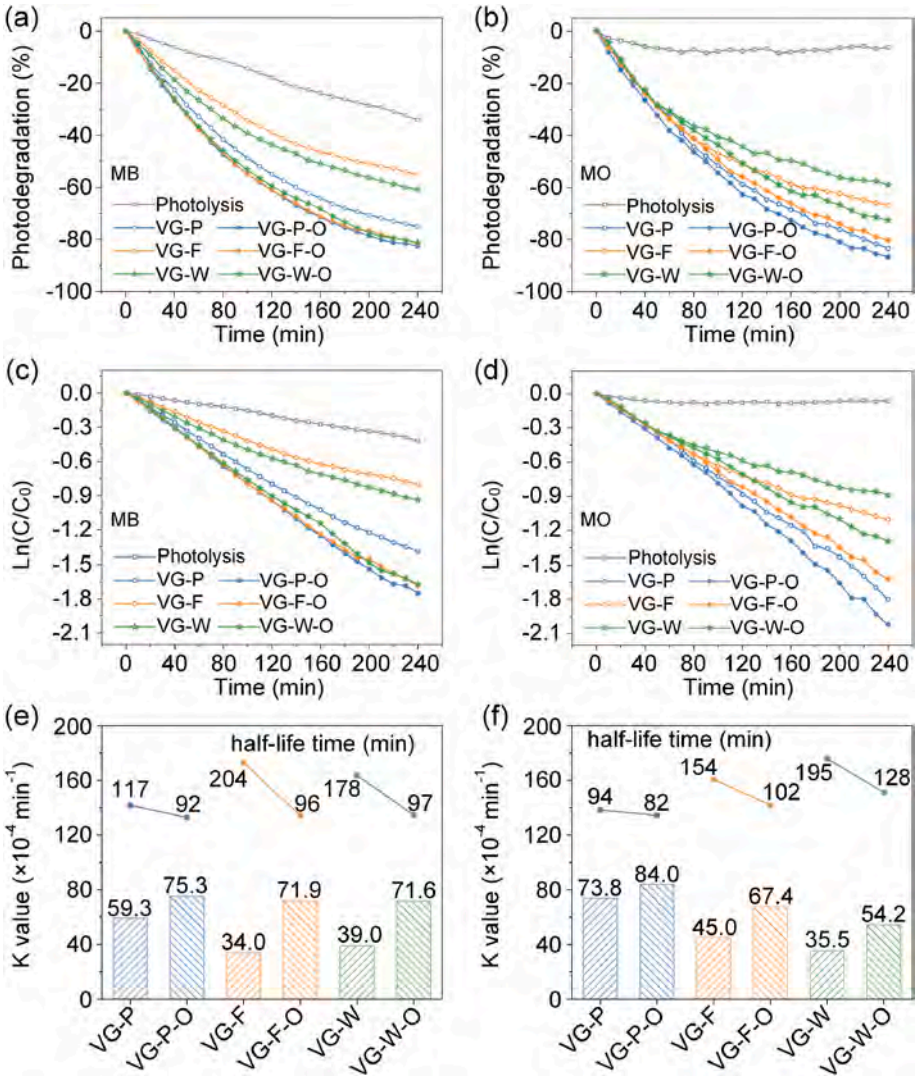

Fig. 4. Photodegradation efficiency of the VG films with different morphologies for MB (a) and MO (b). The kinetic ratio evaluation of the K value of the MB (c) and MO (d) dyes. The photodegradation rate and the half-life time of the VG films for MB (e) and MO (f) degradation.

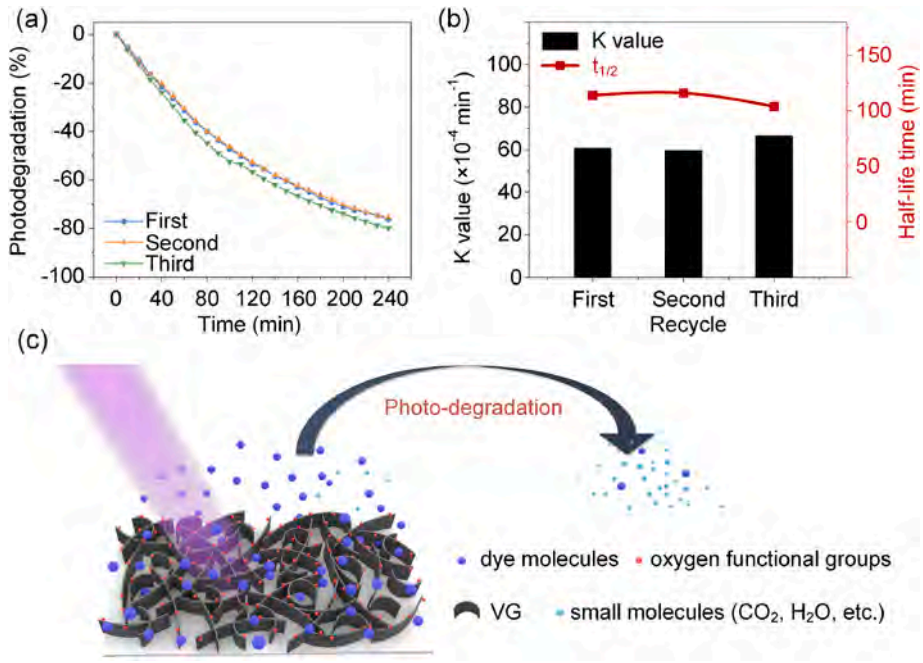

Fig. 5. Recycle test of VG-P-O for MB (a) and the corresponding photodegradation rate and half-life time (b). The schematic illustration for the degradation process (c).

instantly. This result indicates the hydrophobic nature of the VG films can be changed to hydrophilic by the oxygen plasma treatment, which will promote the contact of the VG film surface with the pollution solution thereby facilitating the photodegradation.

3.2. Photodegradation characterizations

The cationic MB and anionic MO dyes are utilized to characterize the photocatalysis capability of the VG films under UV stimuli. Fig. 3 shows the absorbance variation of MB and MO over time under the catalysis of the VG films. The diminishing absorbance intensity, which confirms by the decreasing concentration of dyes in Fig. S2, indicates that the photodegradation process takes place with the VG catalysts. Besides, Fig. 4a presents the relative changes of the concentration of aqueous MB solutions over time, with an initial MB concentration of 5 mg L^{-1}. The self-degradation under the UV stimuli is observed in the MB solution without VG catalyst that only 34.2% are degraded after 4 h, which is similar to the reported value [5]. The self-degradation can be ascribed to the photolysis of MB under the UV explosion [17]. By utilizing the VG films as the photocatalyst, the degradation is greatly enhanced. Impressively, the degradation strongly depends on the VG morphology, where the VG-P, VG-F, and VG-W exhibit high degradation of 75.0%, 55.2%, and 60.8%, respectively. It is reasonable that the relatively denser porous structure of the VG-P can provide a much larger active surface area for contacting the pollutants and processing the degradation reaction [18,19], resulting in a better degradation efficiency. Moreover, the degradation has been further promoted after the oxygen plasma treatment that the VG-P-O exhibited a degradation efficiency of 82.6%, higher than that of VG-P. Impressively, the degradation of the VG-F-O and VG-W-O also increases to 81.4% and 81.2%, respectively. Meanwhile, a similar degradation performance is obtained for the anionic dye, MO, that the VG-P provides the highest degradation efficiency of 83.4% yet the VG-F and VG-W show relatively lower degradation efficiencies of 66.8% and 59.0%, respectively. Moreover, the increased degradation efficiencies of 86.7%, 80.2%, and 72.6% are obtained from the VG-P-O, VG-F-O, and VG-W-O, respectively.

The photocatalytic kinetic constants are calculated and the results are shown in Table S2 and Fig. 4c and d. According to the Langmuir-Hinselwood kinetic theory, the degradation of MB and MO dyes agrees well with the pseudo-first-order kinetics for all the VG films [20,21]. As shown in Fig. 4e and f, and Table S2, the VG-P-O shows the best catalytic performance that the kinetic constants reach 75.3 × 10^{-4} min^{-1} for MB dye and 84.0 × 10^{-4} min^{-1} for MO dye. On the other hand, the oxygen plasma treatment of the VG films produces a greater promotion on the photodegradation property of MB than that of MO. For example, the kinetic constant increment of VG-F-O is 37.9 × 10^{-4} min^{-1} compared with the VG-F in MB solution, while that is only 22.4 × 10^{-4} min^{-1} in MO solution. It is by virtue of the enhanced adsorption of the positively charged MB molecules on the negatively charged VG surface that stems from the oxygen functional groups introduced by the oxygen plasma treatment. Moreover, as shown in Fig. 4e and f, the $t_{1/2}$ of the VG films declines after the oxygen plasma treatment, among which the VG-P-O shows the shortest $t_{1/2}$ of 92 and 82 min for MB and MO, respectively.

Furthermore, in order to evaluate the recyclability of the VG films, the recycle test of the VG-P-O for MB is conducted for three cycles. As presented in Fig. 5a and b, the photodegradation efficiency, K values and the $t_{1/2}$ maintain very well, indicating the desirable recyclability of the VG catalyst. Impressively, the photodegradation efficiency at the third cycle is slightly enhanced, which is believed to be contributed from the full infiltration of the dye solutions in the VG nanopores.

The photodegradation process is illustrated in Fig. 5c. With the irradiation of light, the electron-hole pairs are generated in the graphene and migrated to the surface, which has the properties of reductibility and oxidability. Afterward, water molecules are oxidized to generate intermediates with high activity, e.g., hydroxyl groups, indiscriminately oxidizing the organic dyes to micromolecules [22,23]. Therefore, the degradation of the organic dyes is strongly influenced by the morphology of the VG films, which determines the active surface area of the VG catalyst. In addition, the function of the oxygen treatment is ascribed to the following reasons: firstly, the etching effect in the oxygen treatment changes the top structures of the VG-F and VG-W thereby exposing thin and sharp flakes so that increase the active surface area. Secondly, the wettability of the VG is greatly enhanced after the oxygen plasma treatment, thus improving the accessibility of the VG for the dye molecules in the solution. Thirdly, the defects and oxygen functional groups induced by the oxygen treatment provide more active sites for

catalyzing. As a result, the degradation capability of the VG films is greatly enhanced by the oxygen plasma treatment. Furthermore, MB, as a cationic dye, may electrostatically absorb on the negatively charged VG nanosheets raised by the oxygen functional groups, owing to the electrostatic interaction, which is believed to enhance the degradation efficiency [24]. Hence, the degradation efficiency increment after oxygen treatment is more effective for cationic than anionic dyes.

4. Conclusion

In this work, the VG films with three different morphologies, VG-P, VG-F, and VG-W, are prepared by a PECVD process with controlled growth conditions. The VG films show desirable photocatalytic properties that are strongly dependent on the morphologies. Benefitting from the porous structure, a large active surface is obtained in the VG-P, which exhibits the best photocatalytic capability. Furthermore, the oxygen plasma treatment is utilized to induce oxygen functional groups that tune the VG films from hydrophobic to hydrophilic, thereby enhancing the photocatalytic performance of the VG films. As a result, the treated VG-P-O shows the highest photodegradation efficiency of 82.6% for MB and 86.7% for MO. On the other hand, the oxygen plasma treatment also changes the morphologies of VG-F and VG-W that exposes sharp edges. Therefore, the treated VG-F and VG-W show an enhanced degradation efficiency of 81.4% and 81.2% for MB and 80.2% and 72.6% for MO, respectively. This investigation on the morphology and surface engineering of the VG photocatalyst has a guiding significance for the design of the carbon-based photocatalyst for environmental remediation applications.

Author contributions

J. R. conducted the experiments. J. R. and M. W. wrote the manuscript with input from all coauthors. J. H. conceived the idea. Y. M., J. S. and X. C. supervised the project. Z. T., L. X., and S. J. participated in revising the manuscript. All authors have read and agreed to the published version of the manuscript.

Declaration of competing interest

The authors declare that they have no known competing financial interests or personal relationships that could have appeared to influence the work reported in this paper.

Acknowledgement

This research was supported by the National Key R&D Program of China (Grant No. 2017YFA0304203), the National Natural Science Foundation of China (Grants No. 21805174 and 51902190), the Key Research and Development Program of Shanxi Province for International Cooperation (201803D421082), Scientific and Technological Innovation Programs of Higher Education Institutions in Shanxi (2019L0013 and 2019L0018), research project supported by Shanxi Scholarship Council of China (2021-004), the 111 Project (Grant No. D18001), the Changjiang Scholars and Innovative Research Team at the University of Ministry of Education of China (Grant No. IRT_17R70), and the Fund for Shanxi “1331 Project”.

Appendix A. Supplementary data

Supplementary data to this article can be found online at https://doi.org/10.1016/j.ceramint.2021.12.145.

References

[1] G. Yildiz, M. Bolton-Warberg, F. Awaja, Graphene and graphene oxide for biosensing: general properties and the effects of graphene ripples, Acta Biomater. 131 (2021) 62–79, https://doi.org/10.1016/j.actbio.2021.06.047.
[2] X. Huang, X. Qi, F. Boey, H. Zhang, Graphene-based composites, Chem. Soc. Rev. 41 (2012) 666–686, https://doi.org/10.1039/c1cs15078b.
[3] S. Zhang, H. Wang, J. Liu, C. Bao, Measuring the specific surface area of monolayer graphene oxide in water, Mater. Lett. 261 (2020) 127098, https://doi.org/10.1016/j.matlet.2019.127098.
[4] B.K. Sahu, R.N. Juine, M. Sahoo, R. Kumar, A. Das, Interface of GO with SnO_2 quantum dots as an efficient visible-light photocatalyst, Chemosphere 276 (2021) 130142, https://doi.org/10.1016/j.chemosphere.2021.130142.
[5] A. Guirguis, S.R. Polaki, G. Sahoo, S. Ghosh, M. Kamruddin, A. Merenda, X. Chen, J.W. Maina, G. Szekely, L. Dumee, Engineering high-defect densities across vertically-aligned graphene nanosheets to induce photocatalytic reactivity, Carbon 168 (2020) 32–41, https://doi.org/10.1016/j.carbon.2020.05.058.
[6] J. Nong, W. Wei, X. Song, L. Tang, J. Yang, T. Sun, L. Yu, W. Luo, C. Li, D. Wei, Direct growth of graphene nanowalls on silica for high-performance photoelectrochemical anode, Surf. Coating. Technol. 320 (2017) 579–583, https://doi.org/10.1016/j.surfcoat.2016.10.092.
[7] D.A.C. Brownson, A.G. Ferrari, S. Ghosh, M. Kamruddin, J. Iniesta, C.E. Banks, Electrochemical properties of vertically aligned graphenes: tailoring heterogeneous electron transfer through manipulation of the carbon microstructure, Nanoscale Adv 2 (2020) 5319–5328, https://doi.org/10.1039/d0na00587h.
[8] M. Ghosh, V. Anand, M.R. Gowravaram, Wetting characteristics of vertically aligned graphene nanosheets, Nanotechnology 29 (2018) 385703, https://doi.org/10.1088/1361-6528/aad157.
[9] Y. Li, C. Ai, S. Deng, Y. Wang, X. Tong, X. Wang, X. Xia, J. Tu, Nitrogen doped vertical graphene as metal-free electrocatalyst for hydrogen evolution reaction, Mater. Res. Bull. 134 (2021) 111094, https://doi.org/10.1016/j.materresbull.2020.111094.
[10] M. Wang, Y. Ma, Nitrogen-doped graphene forests as electrodes for high-performance wearable supercapacitors, Electrochim. Acta 250 (2017) 320–326, https://doi.org/10.1016/j.electacta.2017.08.073.
[11] J. Han, M. Wang, Z. Tong, Y. Ma, Triboelectric nanogenerator based on graphene forest electrodes, J. Inorg. Mater. 34 (2019), https://doi.org/10.15541/jim20180521.
[12] Y. Ma, W. Jiang, J. Han, Z. Tong, M. Wang, J. Suhr, X. Chen, L. Xiao, S. Jia, H. Chae, Experimental investigation on vertically oriented graphene grown in a plasma-enhanced chemical vapor deposition process, ACS Appl. Mater. Interfaces 11 (2019) 10237–10243, https://doi.org/10.1021/acsami.9b00896.
[13] Y. Ma, M. Wang, N. Kim, J. Suhr, H. Chae, A flexible supercapacitor based on vertically oriented ‘Graphene Forest’ electrodes, J. Mater. Chem. 3 (2015) 21875–21881, https://doi.org/10.1039/c5ta05687j.
[14] J. Han, Y. Ma, M. Wang, L. Li, Z. Tong, L. Xiao, S. Jia, X. Chen, Oxygen-assisted trimming growth of ultrahigh vertical graphene films in a PECVD process for superior energy storage, ACS Appl. Mater. Interfaces 13 (2021) 12400–12407, https://doi.org/10.1021/acsami.1c00544.
[15] J. Rafiee, X. Mi, H. Gullapalli, A.V. Thomas, F. Yavari, Y. Shi, P.M. Ajayan, N. A. Koratkar, Wetting transparency of graphene, Nat. Mater. 11 (2012) 217–222, https://doi.org/10.1038/nmat3228.
[16] J. Li, Z. Liu, Q. Guo, S. Yang, A. Xu, Z. Wang, G. Wang, Y. Wang, D. Chen, G. Ding, Controllable growth of vertically oriented graphene for high sensitivity gas detection, J. Mater. Chem. C 7 (2019) 5995–6003, https://doi.org/10.1039/c9tc01246j.
[17] S. Chatterjee, A.K. Kar, Oxygen-vacancy-dependent photocatalysis for the degradation of MB dye using UV light and observation of Förster resonance energy transfer (FRET) in PANI-Capped ZnO, J. Phys. Chem. C 124 (2020) 18284–18301, https://doi.org/10.1021/acs.jpcc.0c03248.
[18] M. Nawaz, W. Miran, J. Jang, D.S. Lee, One-step hydrothermal synthesis of porous 3D reduced graphene oxide/TiO_2 aerogel for carbamazepine photodegradation in aqueous solution, Appl. Catal., B 203 (2017) 85–95, https://doi.org/10.1016/j.apcatb.2016.10.007.
[19] C. Hou, Q. Zhang, Y. Li, H. Wang, P25-graphene hydrogels: room-temperature synthesis and application for removal of methylene blue from aqueous solution, J. Hazard Mater. 205–206 (2012) 229–235, https://doi.org/10.1016/j.jhazmat.2011.12.071.
[20] G.S. Das, J.P. Shim, A. Bhatnagar, K.M. Tripathi, T. Kim, Biomass-derived carbon quantum dots for visible-light-induced photocatalysis and label-free detection of Fe (III) and ascorbic acid, Sci. Rep. 9 (2019) 15084, https://doi.org/10.1038/s41598-019-49266-y.
[21] W. Liu, Y. Li, F. Liu, W. Jiang, D. Zhang, J. Liang, Visible-light-driven photocatalytic degradation of diclofenac by carbon quantum dots modified porous g-C_3N_4: mechanisms, degradation pathway and DFT calculation, Water Res. 151 (2019) 8–19, https://doi.org/10.1016/j.watres.2018.11.084.
[22] Y. Xu, W. Lin, H. Wang, J. Guo, D. Yuan, J. Bao, S. Sun, W. Zhao, C. Zhao, Dual-functional polyethersulfone composite nanofibrous membranes with synergistic adsorption and photocatalytic degradation for organic dyes, Compos. Sci. Technol. 199 (2020) 108353, https://doi.org/10.1016/j.compscitech.2020.108353.
[23] L. Lu, R. Shan, Y. Shi, S. Wang, H. Yuan, A novel TiO_2/biochar composite catalysts for photocatalytic degradation of methyl orange, Chemosphere 222 (2019) 391–398, https://doi.org/10.1016/j.chemosphere.2019.01.132.
[24] G.K. Ramesha, A.V. Kumara, H.B. Muralidhara, S. Sampath, Graphene and graphene oxide as effective adsorbents toward anionic and cationic dyes, J. Colloid Interface Sci. 361 (2011) 270–277, https://doi.org/10.1016/j.jcis.2011.05.050.